Earth and Planetary Science Letters 514 (2019) 1–12

Contents lists available at ScienceDirect

Earth and Planetary Science Letters

www.elsevier.com/locate/epsl

Topographic evolution of the western United States since the early Miocene

Quan Zhou, Lijun Liu *

Department of Geology, University of Illinois at Urbana-Champaign, United States of America

ARTICLE INFO

Article history:
Received 7 June 2018
Received in revised form 22 January 2019
Accepted 21 February 2019
Available online xxxx
Editor: J.P. Avouac

Keywords:
western United States topography
gravity anomaly
residual topography
dynamic uplift
intruding pacific mantle
paleotopography

ABSTRACT

The origin of the high topography within the western United States has been attributed to either crustal/lithospheric isostasy or dynamic topography, but their relative contributions remain unconstrained. Here we investigate this problem using gravity, residual topography and geodynamic modeling. We first evaluate two end-member scenarios of isostatic balance: crustal isostasy and lithospheric isostasy. Both cases lead to prominent negative mantle residual gravity within the tectonically active western U.S. and unrealistic crustal/lithospheric density structures, requiring the presence of low-density mantle underneath. The negative mantle residual gravity is consistent with both the estimated positive residual topography and calculated dynamic uplift due to the presence of hot asthenospheric mantle underneath. Geodynamic modeling further reveals that this landward migrating dynamic uplift originates from the eastward intrusion of the hot Pacific mantle through tears and edges of the Juan de Fuca slab since middle Miocene. The estimated paleotopography maps by combining dynamic topography and lithosphere isostasy over the western U.S. are consistent with several observational constraints, including episodic uplifts of the Sierra Nevada, post-mid-Miocene uplift of the Idaho batholith, the sustaining subsidence within most of the B&R, and the largely stable topography of central Colorado Plateau since 20 Ma.

1. Introduction

Earth's surface topography reflects both isostatic adjustment of variable crustal and/or lithospheric structures (density and thickness) and dynamic response of the convecting sub-lithospheric mantle (Braun, 2010; Flament et al., 2013; Liu, 2015). However, the respective contributions of isostasy (hereafter referring to compensation within either the crust or the lithosphere) and dynamic topography remain elusive, as is due to imperfect knowledge about lithosphere and sub-lithospheric mantle dynamic properties. For example, debates exist regarding the respective contributions of isostasy and mantle convection on Earth's long-wavelength topography (Hoggard et al., 2016, 2017; Yang and Gurnis, 2016; Yang et al., 2017). At shorter wavelength, similar uncertainties remain on the topographic origin of continents, especially that of high topography regions, such as southern Africa (Lithgow-Bertelloni and Silver, 1998; Flament et al., 2013; Molnar et al., 2015; Hu et al., 2018) and western North America (Hasterok and Chapman, 2007; Flowers, 2010; Forte et al., 2010; Liu and Gurnis, 2010; Karlstrom et al., 2012; Liu and Hasterok, 2016)).

Here we investigate the origin and evolution of topography within the western United States (U.S.) since the early Miocene. In this case, residual topography, i.e., observed topography subtracted by isostatic topography, is used as an analogy for dynamic topography. The western U.S. has an overall high (1–2 km elevation) topography (Fig. 1a) and thin (30–45 km) crust (Fig. 2a). This precludes the adoption of Airy isostasy (due to crustal thickness variation) in explaining its topography. Consequently, several alternative hypotheses have been proposed. Becker et al. (2014) attributed positive residual topography within the Basin & Range (B&R) to dynamic topography. Levandowski et al. (2014) used a similar method as in Becker et al. (2014) but concluded that lithospheric isostasy is sufficient to explain the western U.S. high topography. Schmandt et al. (2015) proposed that Pratt isostasy (due to lateral crustal density variation) could account for the topographic contrast between the western and eastern U.S.

The challenge in deciphering the origin of present-day topography resides in the additive nature of different topographic mechanisms. We suggest that this problem could be better addressed if we further (1) test different end-member scenarios using complementary data constraints like gravity (Fig. 1b), and (2) deconvolve

* Corresponding author.
E-mail address: ljliu@illinois.edu (L. Liu).

https://doi.org/10.1016/j.epsl.2019.02.029
0012-821X/

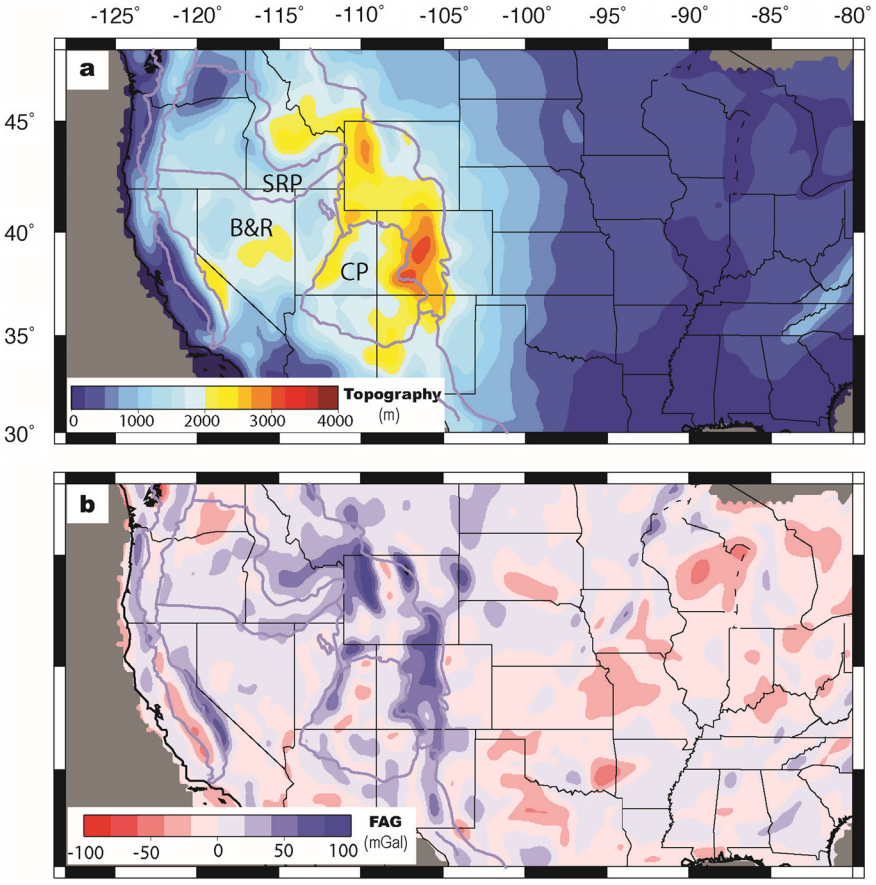

Fig. 1. a) Topography for continental U.S. from ETOPO 1.0 and low-pass filtered at 200 km wavelength. Major tectonic provinces of the western U.S. are shown with gray outlines. SRP: Snake River Plain, B&R: Basin & Range, CP: Colorado Plateau. **b**) Free air gravity anomalies for the same region from EGM 2012 and also filtered to above 200 km wavelength. (For interpretation of the colors in the figure(s), the reader is referred to the web version of this article.)

different mechanisms by unfolding their temporal evolution via geodynamic modeling (e.g., Liu, 2015). For (1), we evaluate the hypotheses of crustal and lithospheric isostasy by comparing their respective gravity implication with that observed. This could illuminate on whether dynamic topography is required. For (2), we first estimate the necessary residual topography and then investigate its relationship with the temporally varying dynamic topography through a recently established mantle convection model that matches several independent observations, including the history of intraplate volcanism (Zhou et al., 2018a) and the formation of the peculiar seismic anisotropy over the western U.S. (Zhou et al., 2018b).

As discussed later, the purely isostatic model, no matter compensated within the crustal or lithospheric depths, always leads to negative isostatic residual gravity anomalies within the tectonically active region, consistent with the existence of low-density upper mantle underneath. We also find that the apparently different conclusions regarding the nature of western U.S. topography between Levandowski et al. (2014) and Becker et al. (2014) are likely due to their different assumptions of lithospheric thickness, which, in the former study, was a constant 150 km and, the latter, inferred from receiver functions. Consequently, we further estimate the amount of the present-day residual topography from both crustal and lithospheric isostatic assumptions (e.g., Becker et al., 2014), and investigate its dynamic origin and temporal evolution using a recently developed mantle convection model. Finally, we provide an estimated paleotopography history of the western U.S. since the early Miocene by combining the modeled dynamic topography with isostatic topography associated with the lithospheric extension of the region, and evaluate this result against several available observational constraints.

2. Methods

The proposed research involves several types of calculations: gravity anomaly, residual topography, and dynamic topography. This section discusses their respective methodology. In all the calculations, to remove the potential effects of flexure, we low-pass filtered all quantities with a cut-off wavelength of 200 km using a Gaussian filter.

2.1. Gravity calculation

To evaluate the consistency of recent isostasy models with gravity, we consider two end-member scenarios: crustal and lithospheric isostasy. For the observed surface topography, the former scenario, where density anomalies are placed at a shallow depth, maximizes the gravity effect of non-isostatic mass anomalies. The latter scenario, by placing density anomalies at a greater depth, captures the lower bound of this gravity effect. Collectively, these two cases help to examine whether the observed topography could be solely due to isostasy. For simplicity, we assume that surface topography is supported by a layer of laterally varying density distribution in either case.

For the former scenario, a two-layer reference continental crust is considered (e.g., Schmandt et al., 2015). The upper crust (UC) has a reference density of 2600 kg/m^3 and a thickness of 15 km, while the lower crust (LC) has a reference density of 2850 kg/m^3 and a thickness of 22 km. This reference crust, whose surface is assumed

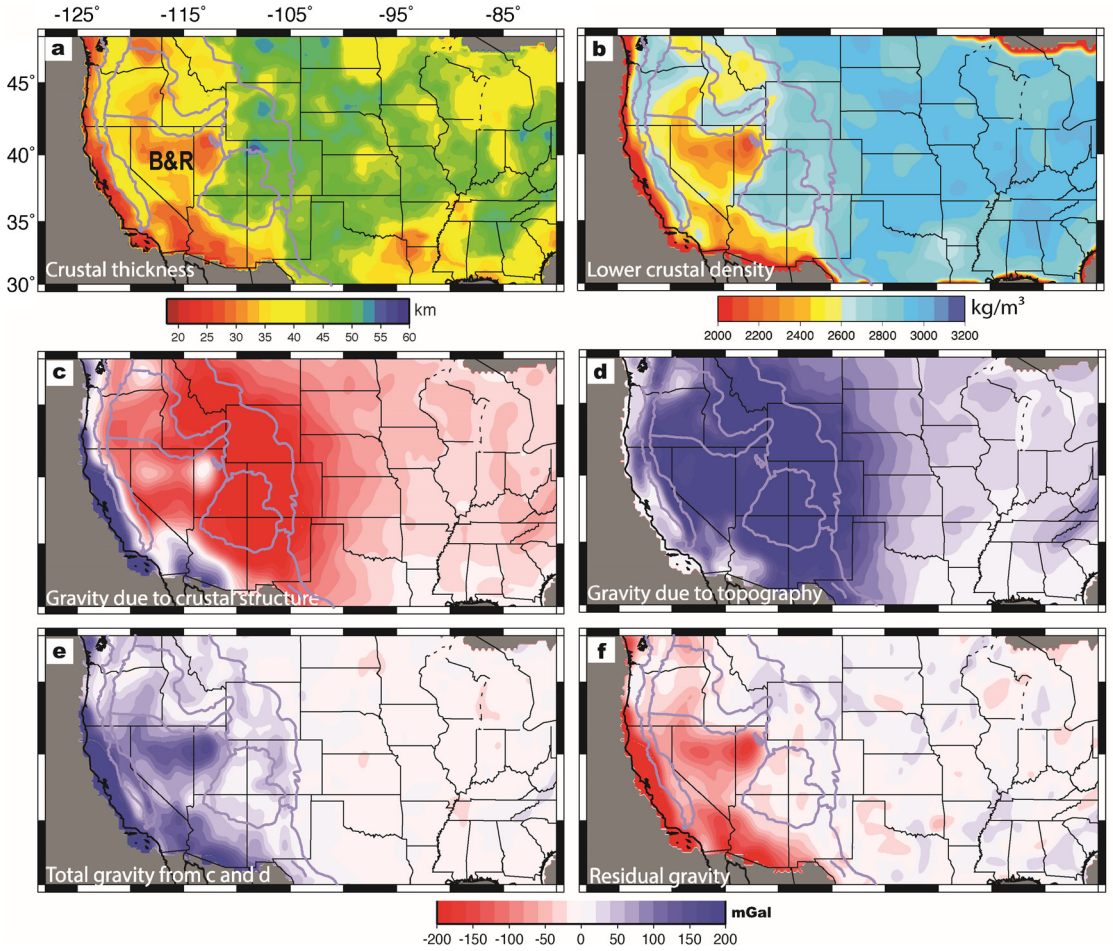

Fig. 2. Gravity test for the case of crustal isostasy. The results are filtered to above 200 km wavelength. **a**) Crust thickness from Schmandt et al. (2015), which ranges from 25 km to 55 km. **b**) Inferred lower crustal density that ranges from 2200 kg/m^3 to 2900 kg/m^3, where the density beneath the B&R is unreasonably low. **c**) Gravity anomaly due to crust density anomaly and Moho depth variation. The western U.S. is overall negative due to its low crustal density. **d**) Gravity anomaly due to topography. **e**) Summation of **c** and **d**. **f**) Residual mantle gravity anomaly calculated by subtracting **e** from observation Fig. 1b. This reflects gravity effects due to mantle density anomalies. The B&R has negative values, indicating low-density mantle underneath.

to be at sea-level, sets the basis for continental-scale variations of gravity anomalies. The fact that the regional average of calculated gravity anomalies is close to zero (e.g., Fig. 2f) supports this choice of reference. Since we are evaluating the lateral variation of residual gravity signals instead of their regional average, which is dependent on the choice of the reference level, we could adjust the reference crustal thickness in cases when the regional average of gravity residuals obviously deviates from zero. More details of the model parameters for this section are included in Supplementary Table 1.

In the crustal isostasy case, crustal isostasy assumes that the observed topography is fully supported by the crust. Assuming a two-layer density structure as that in Schmandt et al. (2015), the observed east-west topography contrast of the U.S. continent is attributed to varying LC density (Fig. 2b). In practice, we infer the local LC thickness by subtracting a constant UC thickness (15 km) from the observed Moho depth (Schmandt et al., 2015). We subsequently vary the LC density to match surface topography. Then we compute the total free-air gravity anomaly due to both surface and Moho topographies (Fig. 2d), as well as that due to inferred crustal density variations (Fig. 2c). Finally, we subtract the total predicted free-air gravity anomaly (Fig. 2e) from that observed (Fig. 1b) to obtain the residual gravity anomaly (Fig. 2f), which represents the mantle contribution.

For the latter scenario of lithospheric isostasy, we assume that the observed topography is isostatically compensated above the lithosphere–asthenosphere boundary (LAB) (Pasyanos et al., 2014; Fig. 3a). The crust in this case is similar to that used in the former scenario, except that the lower crust has a constant density at 2850 kg/m^3. We vary the mantle lithosphere density laterally (Fig. 3b) within the seismically determined lithosphere thickness (Fig. 3a), in order to achieve the observed topography. Again, we compute the residual gravity anomaly from this exercise (Fig. 3c–e) and estimate the required mantle contribution due to its lateral density variation. For the purpose of completeness, we also repeat this exercise by assuming compensation at a shallower depth around the mid-lithosphere discontinuity (MLD), i.e., 70–100 km depth beneath the continental U.S. (Hansen et al., 2015; Fig. S1).

We emphasize that because the observed surface topography is assumed to be isostatically balanced in both scenarios, any non-zero residual gravity signal calculated here should reflect the uncounted effect of mantle density heterogeneity. Further quantification of this additional density anomaly will require iteratively solving for its dynamic topography contribution as well, an exercise that may not guarantee a unique solution. Therefore, our main purpose of doing these calculations is to test the validity of the two existing isostasy hypotheses, which, if correct, should result in negligible residual gravity anomalies. Any non-zero residual gravity, especially over regional scales as shown below, should illuminate deeper mantle dynamic effects.

We developed an MPI-parallel code to compute the gravity anomaly (relative to the reference level, i.e., sea surface) for a given

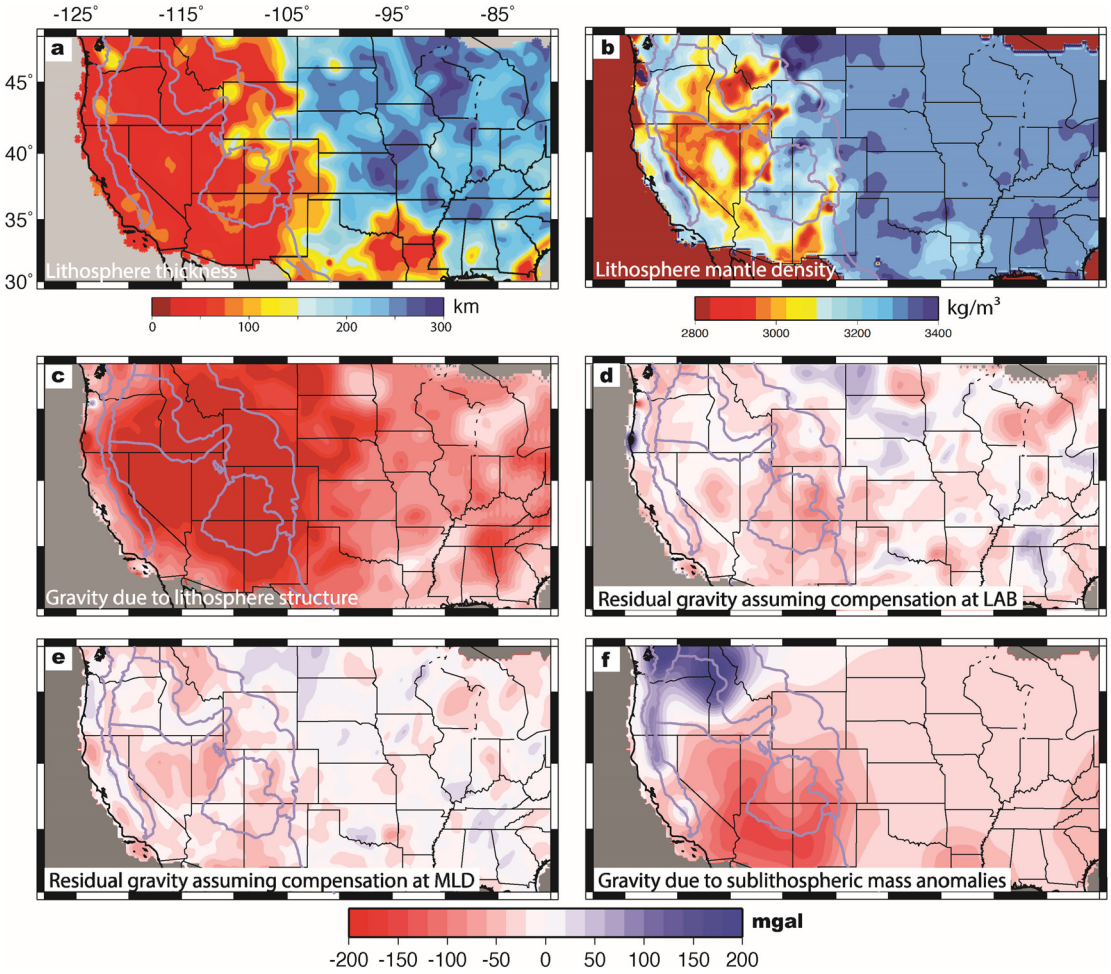

Fig. 3. Gravity test for the case of lithosphere isostasy. The results are filtered to above 200 km wavelength. **a**) Lithosphere thickness from Pasyanos et al. (2014), that ranges from 60 km to 140 km, correlated with the crust thickness. Note the unreasonably thin CP lithosphere in this model. **b**) Inferred mantle lithosphere density that ranges from 2800 kg/m^3 to 3400 kg/m^3. **c**) Gravity anomaly due to mantle lithosphere density, Moho depth, and lithosphere thickness variations. **d**) Residual gravity anomaly by subtracting the total lithospheric gravity effect from that observed in Fig. 1b; this reflects gravity effects due to sub-lithospheric mantle density anomalies. **e**) Same as **d**, but assuming isostatic compensation at the mid-lithospheric discontinuity (more details in Fig. S1). **f**) Predicted gravity anomaly due to the sub-lithosphere mantle density structure converted from tomography. Note the similar location of negative gravity anomaly over the western U.S. in **d**–**f**.

density structure (topography is treated as a lateral density variation) by computing the integral:

$$g = \int \frac{G\Delta\rho}{r^2} dV \tag{1}$$

G is the gravitational constant, $\Delta\rho$ is the density anomaly, V is the integration volume, r is the distance between the density element and the observation point.

2.2. Residual topography calculation

As stated above, the compensation depth can be assumed either at the Moho or the LAB, depending on the adopted isostasy hypothesis. We consider both cases in estimating the residual topography of the western U.S. (Fig. 4). Since this calculation involves the force balance on a global scale, the choice of reference topography would matter. Here, we follow the two recent studies on western U.S. residual topography (Becker et al., 2014; Levandowski et al., 2014) that considered the mid-ocean ridge depth as the global reference. Other parts of the calculation also follow those of Becker et al. (2014): the continental crust has a uniform density of 2836 kg/m^3, and the asthenospheric mantle has a density of 3237 kg/m^3. The crustal density is the average value of CRUST 2.0, and the asthenospheric mantle density is inferred by minimizing the average difference between predicted and observed topography. The only difference in this study is that we further treat the topography of the Snake River Plain (SRP), due to its strong relevance to our recent geodynamic model (Zhou et al., 2018a). The lower-than-ambient elevation of SRP should be due to its basalt-rich crust (McCurry and Rodgers, 2009; DeNosaquo et al., 2009). The mass of the SRP crust has been estimated to be equivalent to a 14-km thick layer of gabbro (McCurry and Rodgers, 2009), similar to a conclusion based on gravity, tomography, and heat flow (DeNosaquo et al., 2009). Based on these earlier studies, we estimate the SRP crustal density to be ~2950 kg/m^3 by largely removing its surface topography relative to its surrounding regions.

In the case of crustal isostasy, we compute the isostatic topography based on the following formula:

$$t = \frac{\rho_a - \rho_c}{\rho_a} l_c + t_o \tag{2}$$

where ρ_a is mantle density, ρ_c is continental crust density, l_c is the observed crustal thickness, t_o is the mid-ocean ridge depth, i.e. −2.6 km (Carlson and Johnson, 1994).

In the case of lithospheric isostasy, the isostatic topography is computed as:

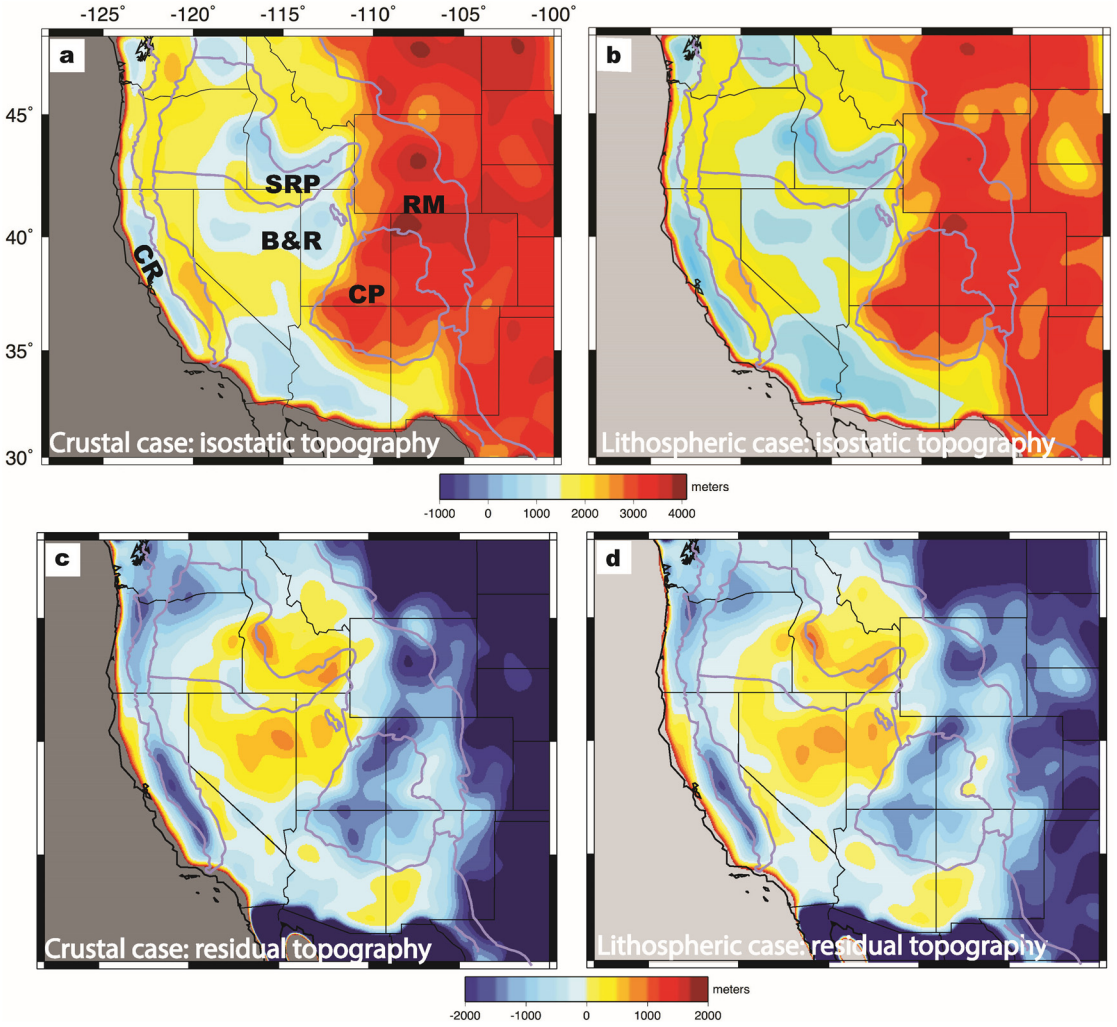

Fig. 4. Isostatic (upper) and residual (lower) topography for two end-member isostasy scenarios. **a**) The isostatic topography for crustal isostasy. The Basin and Range is low isostatically, while the Colorado Plateau, Cascadia mountains, and cratonic North America are high. **b**) Same as **a** but for lithospheric isostasy. **c**) The residual topography for crustal isostasy that largely mirrors the isostatic topography. **d**) The residual topography for lithospheric isostasy that also mirrors its corresponding isostatic topography.

$$t = \frac{\rho_a - \rho_c}{\rho_a} l_c + \frac{\rho_a - \rho_l}{\rho_a} l_l + t_o \tag{3}$$

where ρ_l is mantle lithosphere density, l_l is the thickness of mantle lithosphere constrained by observed LAB depth subtracting observed Moho depth.

For both cases, the residual topography is defined as the observed topography subtracted by the isostatic topography.

2.3. Mantle convection model

Our time-dependent mantle convection model is based on a hybrid approach of data assimilation. Here we provide a summary about this approach, and more details could be found in Zhou and Liu (2017) and Zhou et al. (2018a). The hybrid approach has two parts: forward and adjoint data assimilation.

In the forward data assimilation, the mantle is approximated as an incompressible Stokes fluid, with three governing equations:

$$\nabla \cdot \vec{u} = 0 \tag{4}$$

$$\nabla P + \nabla \cdot (\eta \nabla \vec{u}) = \rho_m \alpha \Delta T \vec{g} \tag{5}$$

$$\frac{\partial T}{\partial t} + \vec{u} \cdot \nabla T = \kappa \nabla^2 T \tag{6}$$

where $\vec{u}$ is velocity, P, dynamic pressure, η, dynamic viscosity, ρ_{m}, reference mantle density, α, thermal expansion coefficient, ΔT, temperature anomaly, κ, thermal diffusivity, and $\vec{g}$, gravitational acceleration.

The forward part assimilates past plate motions (Müller et al., 2008) as the velocity boundary condition and reconstructed seafloor ages to update the thermal profiles of oceanic lithosphere (Liu and Stegman, 2011). A major problem for the forward data assimilation is that it does not have a well-constrained initial condition. Therefore, the adjoint data assimilation is introduced to address this problem.

The adjoint data assimilation updates the initial condition of a model by 'forcing' the predicted present-day mantle thermal state to match that observed through an iterative forward-adjoint scheme (e.g. Bunge et al., 2003; Liu and Gurnis, 2008). In practice, the method starts with a first guess of the initial condition. Then a forward simulation generates a present-day mantle structure, which is compared with that converted from tomography (Sigloch, 2011; Schmandt and Lin, 2014). The difference between the prediction and observation (i.e., the residual temperature field) is integrated back to the initial time to correct the initial condition. The adjoint equations for backward transporting the mismatch field is as follows (Liu and Gurnis, 2008):

$$\frac{\delta J}{\delta T} = \int_V \left(\frac{\partial \lambda}{\partial t} + \vec{u} \cdot \nabla \lambda + \kappa \nabla^2 \lambda \right) dv \tag{7}$$

$$J = \int_V (T_p - T_d)^2 dv \tag{8}$$

where J is the cost functional to be minimized, λ, the adjoint temperature, $\vec{u}$, velocity, T_P, the predicted temperature field at the present day, T_d, the reference temperature field, and κ, thermal diffusivity. This forward–backward scheme is operated iteratively until a good match on present-day structure is reached.

We apply this approach to a 3D model domain spanning 210°–310° in longitude, 10°–70° in latitude and 2890 km in depth, much broader than the western U.S., to minimize edge effects. The tomography is converted to an effective temperature field to serve as the reference state for the adjoint data assimilation. We use the P-wave model of Schmandt and Lin (2014) to define the upper 1000-km mantle structure below the U.S. and use Sigloch (2011) to approximate regions beyond, with a smooth transition along their boundaries. The differences between the P- and S-wave models of Schmandt and Lin (2014) are minor in resolving the relevant mantle structures for this study.

In this approximated present-day thermal structure, the main uncertain dynamic quantity is the density anomaly associated with the hot mantle below the western U.S., since it cannot be directly derived from the subduction history and is insensitive to the intraplate volcanic history (Zhou et al., 2018a). We therefore further validate the converted temperature structure by comparing its resulting gravity anomaly with the isostatic residual gravity derived from section 2.1. Since it is impossible to uniquely invert for density purely based on gravity, we look for a mantle density structure converted from tomography that does not violate the gravity constraint.

3. Results

In this section, we present several results pertinent for constraining the dynamic vs. isostatic nature of the western U.S. topography. In section 3.1, we show that neither crustal isostasy nor lithospheric isostasy produces non-negligible free-air gravity anomaly within the western U.S. This is consistent with the existence of positive residual topography beneath the region, whose quantification is the focus of section 3.2. Finally, in section 3.3, we show that this residual topography represents dynamic topography originating from the hot sub-lithospheric mantle below the thin lithosphere of the western U.S. Section 3.3 also presents the spatiotemporal evolution of this dynamic topography. In Section 3.4, we present a set of paleotopography maps for the western U.S. by combining the dynamic topography with a recently published compilation on isostatic topography evolution since 20 Ma.

3.1. Gravity constraints on the state of isostasy

In the case of crustal isostasy (e.g., Schmandt et al., 2015), due to the thin crust of the B&R (Fig. 2a), an unreasonably small density (down to 2200 kg/m^3) of the lower crust within large areas of the western U.S. is required (Fig. 2b) to isostatically support their high surface topography. Furthermore, the gravity anomalies (relative to the reference level, for example, the sea level) associated with crustal density and Moho topography has large negative values (<-100 mGal) over most of the western U.S. (Fig. 2c), but an exception is central B&R, where the locally thin crust brings dense mantle to otherwise crustal depths, leading to weakly negative or even positive gravity anomalies. The combined gravity effect due to surface topography (Fig. 2d) and crustal properties (Fig. 2c) is strongly positive (up to 200 mGal) in the B&R (Fig. 2e). The other regions have smaller-amplitude, positive gravity anomalies. Since the observed free air gravity anomaly is only slightly positive in the B&R (Fig. 1b), the residual mantle gravity (observed free air gravity subtracted by surface and crustal gravity effects) is strongly negative (as much as -200 mGal) here (Fig. 2f), indicating mass deficit below the crust of the B&R region. This analysis largely negates the crustal isostasy hypothesis for explaining the observed high topography. The resulting negative mantle residual gravity anomaly within the B&R requires low-density mantle structures either within or below the lithosphere.

In the case of lithospheric isostasy, since the North American LAB (Fig. 3a) has a similar large-scale pattern (thinner below the western U.S.) as that of the Moho (Fig. 2a), the results have certain similarities to those in the crustal isostasy case. For example, the lowest density of the mantle lithosphere occurs below the B&R (Fig. 3b), whose corresponding gravity anomaly (Fig. 3c) resembles that from the variable LC density case (Fig. 2c). However, since the isostatic compensation occurs at the LAB, much deeper than the Moho, the total gravity anomaly (due to surface topography and lithospheric properties) is slightly closer to observation than that in Fig. 2e. Consequently, the residual gravity anomalies (Fig. 3d) also have smaller magnitudes than, although with a similar pattern to, that of the crustal isostasy case. The negative residual gravity over the western U.S. is more inland compared to that in the crustal isostasy case, i.e. over the CP vs. the B&R. This difference reflects the fact that the CP has a shallow LAB similar to the B&R (Fig. 3a), but its crust is thicker (Fig. 2a). Since the negative residual gravity is strongly influenced by the thin mass layer (Figs. 2, 3), we suggest that the exact location of this negative residual gravity is subject to future research, given that the LAB of the CP may not be sufficiently resolved in the LITHO1.0 model. Indeed, a more recent study (Hansen et al., 2015; Fig. S1) suggests a thicker CP lithosphere.

As an additional confirmation, we further compute the residual gravity by assuming compensation occurs at a shallower depth within central-eastern U.S., following similar steps as discussed above (Fig. S1). In this case, we use the lithosphere interface map from Hansen et al. (2015), where the interface over the western U.S. represents the LAB and that further east represents the MLD (Fig. S1a). Since this interface is at a depth range of 60–160 km, it also marks an intermediate scenario for lithospheric compensation. The residual gravity is shown in Fig. 3e, where the most prominent negative residuals occur to the west and the surrounding of the CP, corresponding to the thin lithospheric layer.

Therefore, neither crustal isostasy nor lithospheric isostasy, given the actual surface topography, could fully explain the observed gravity field. The magnitude of the resulting residual gravity anomaly from the latter case is notably smaller, which seems to imply that lithospheric compensation represents a more reasonable assumption than pure crustal isostasy. However, both the inferred lithospheric density variation (2800–3400 kg/m^3 for LAB compensation and 3150–3400 kg/m^3 for MLD compensation) and the inferred lower crustal density (2200–3000 kg/m^3) are unrealistic. In particular, the lowermost ends of values for both cases are significantly below what is considered acceptable. Consequently, both the unrealistically low densities and the associated negative residual gravity require that some of the low-density mass must be distributed below the lithosphere. The relatively short wavelength ($<$500 km) of these anomalies further suggests that the mass deficit must reside in upper mantle depth, consistent with the shallow slow seismic anomalies below the tectonically active western U.S. (e.g., Schmandt and Lin, 2014).

In order to estimate the sub-lithospheric contribution to the observed gravity field, we forward calculate the gravity anomaly associated with the present-day mantle density structure converted from the seismic tomography based on a combination of those from Schmandt and Lin (2014) and Sigloch (2011) (Fig. 3f). To remove the lithospheric contribution, we assume the part above the LAB is neutrally buoyant. The resulting gravity anomalies are close

to zero over central-eastern U.S., similar to the inferred mantle residual gravity (Figs. 2f, 3d, 3e). There are two prominent gravity anomalies within the western U.S. (Fig. 3f). The positive anomaly in the eastern Washington/north Idaho that is related to the dense subducting slab is inconsistent with the neutral residual gravity in the region. This discrepancy could be reconciled if we assume the seismically fast upper-mantle structure below the region represents a neutrally buoyant relict slab (Schmandt and Humphreys, 2011). The prominent negative gravity anomaly within the central and southern B&R that is associated with the widespread shallow hot mantle (Schmandt and Lin, 2014) largely matches the pattern of that from the residual gravity maps (Figs. 2f, 3d, 3e). We emphasize that comparing the amplitudes of these gravity signals is not entirely meaningful, because results from the end-member isostasy scenarios should be taken as being a qualitative estimate on the missing mass anomalies below the lithosphere. On the other hand, the amplitude of forward-calculated gravity anomaly based on the seismic model (Fig. 3f) could be diminished by further inclusion of the associated dynamic topography (e.g., Hager and Richards, 1989). Therefore, the similarity of gravity patterns between the residual and forward calculations further supports the presence of buoyant asthenospheric material below the tectonically active western U.S.

3.2. Present-day residual topography

As concluded from the above gravity analysis, topography of the western U.S., especially that of the B&R province, is not entirely isostatically supported. The consistent inference of negative residual gravity from the two end-member isostasy calculations implies that positive residual topography, due to non-isostatic mantle mass anomalies, should exist in the region. The fact that a greater compensation depth leads to smaller-in-magnitude long wavelength residual gravity suggests that the long-wavelength topography-controlling density anomaly likely sits below the Moho. Therefore, when estimating the residual topography, we adopt a crust that has uniform density but laterally varying thickness. However, we point out that there is likely no best way to estimate the residual topography, and this study mostly follows previous works (e.g., Becker et al., 2014).

We consider residual topography based on both crustal and lithospheric isostasy. For both cases, the estimated isostatic topography patterns are similar but with the former having slightly higher topography due to its omission of the negatively buoyant mantle lithosphere (Fig. 4a, b). This result is consistent with the earlier study by Becker et al. (2014). The isostatic topography is composed of several distinct regions (Fig. 4a, b), with the B&R and SRP being relatively low ($<$1.5 km), and the Colorado Plateau (CP) and Rocky Mountains (RM) being much higher (up to 4.5 km), correlating with their respective crustal thicknesses. The slightly higher topography between the SRP and B&R across the Idaho boundary is likely due to an inaccurate estimate of the SRP crustal properties. To the east of the CP, residual topography is significantly negative. This may indicate either an improper choice of lithospheric density or the existence of negative dynamic topography, a topic that should warrant additional research.

If a region is under perfect isostasy, its residual topography (surface topography subtracted by isostatic topography) should be zero everywhere. However, the pattern of residual topography (Fig. 4c, d) largely mirrors that of the isostatic topography (Fig. 4a, b). The one based on lithospheric isostasy (Fig. 4d) is very similar to that on crustal isostasy (Fig. 4c). The signals from the former are overall shifted toward the positive side relative to those in the latter, but the differences are very minor. In both cases, regions surrounding the western U.S., such as the RM, CP, and CR (Coastal Range), have negative residual topography as low as -2 km. The B&R has positive residual topography with an average amplitude of $\sim$0.5 km that locally exceeds 1 km (eastern Nevada, western Utah and SRP). This estimated residual topography, on one hand, echoes the results of Becker et al. (2014), and, on the other hand, is consistent with the above gravity analysis that requires buoyant sub-lithosphere mantle below the B&R. Given our inaccurate estimate of the SRP crustal property as discussed above, the isolated high topography regions within the B&R may be all connected in reality, forming regionally extensive positive residual topography.

3.3. Dynamic origin of residual topography and its evolution since 20 Ma

To better constrain the nature of the inferred residual topography, we refer to our recently constructed inverse convection model (Zhou and Liu, 2017). To remove the topographic contribution of the conductive lithosphere, we assume all cold materials above 250 km depth are neutrally buoyant, following the recent estimate on the thickness of the stable North American lithosphere using xenolith and xenocryst thermobarometry (Griffin et al., 2004; Carlson et al., 2005). This means that modeled low topography reflects the effect of sub-lithospheric cold anomalies whose convective motion exerts a downward viscous force on the surface. All seismically slow anomalies at shallow depth, which are voluminous below the western U.S., are treated as being hot and buoyant, since they likely represent the intruding Pacific asthenosphere (Zhou et al., 2018a, 2018b). Therefore, the modeled topography is dynamic in nature. In practice, we apply a free-slip boundary condition at the surface when calculating the dynamic topography from the reconstructed thermal states for a given time step. Although the lithosphere is assumed neutrally buoyant, its high viscosity is preserved.

The predicted dynamic topography at the present day (Fig. 5f) largely resembles the estimated residual topography (Fig. 4c, 4d). In particular, the entire B&R is dynamically uplifted, with the maximum dynamic topography occurring in a broad region centered over the SRP and northern Nevada. Other regions like the Pacific Northwest and Wyoming plateau see prominent negative dynamic topography. The similar spatial patterns between Fig. 5f (0 Ma) and Figs. 4c and 4d suggest that the present-day residual topography reflects mostly dynamic topography. The positive residual topography within the B&R is due to the underlying hot mantle that fuels the intraplate volcanism (Zhou et al., 2018a). The negative residual topography in surrounding areas corresponds to the sinking Juan de Fuca slab and other downwelling features beneath the cratonic lithosphere.

This confirmed the dynamic nature of the present-day positive residual topography, which is mostly restricted to the tectonically active region. It also suggests that the topography would evolve over time. Indeed, the reconstructed temporal history of the shallow hot mantle beneath the western U.S. represents a salient output from the hybrid inverse model (Zhou et al., 2018a). The evolving positive dynamic topography within the B&R (Fig. 5) closely follows the migration of the hot mantle anomaly below the western U.S. (Figs. 6, 7). At 20 Ma, when most of the present-day upper-mantle hot anomalies below the western U.S. were reconstructed back to the Pacific mantle side (Zhou et al., 2018a; Fig. 6a), dynamic topography within the B&R has an almost zero amplitude (Fig. 5a). Meanwhile, there was dominant trench-parallel dynamic subsidence above the down-going Juan de Fuca slab along most of the west coast. This north–south oriented dynamic topography pattern was temporally disrupted at $\sim$16 Ma when the central portion of the downgoing slab tore apart, with large volume of hot mantle intruding beneath the Pacific Northwest (Fig. 6b) and forming the Columbia River flood basalt (CRB); a rapid pulse of dynamic uplift occurred within Washington and Oregon (Fig. 5b). Intrusion of

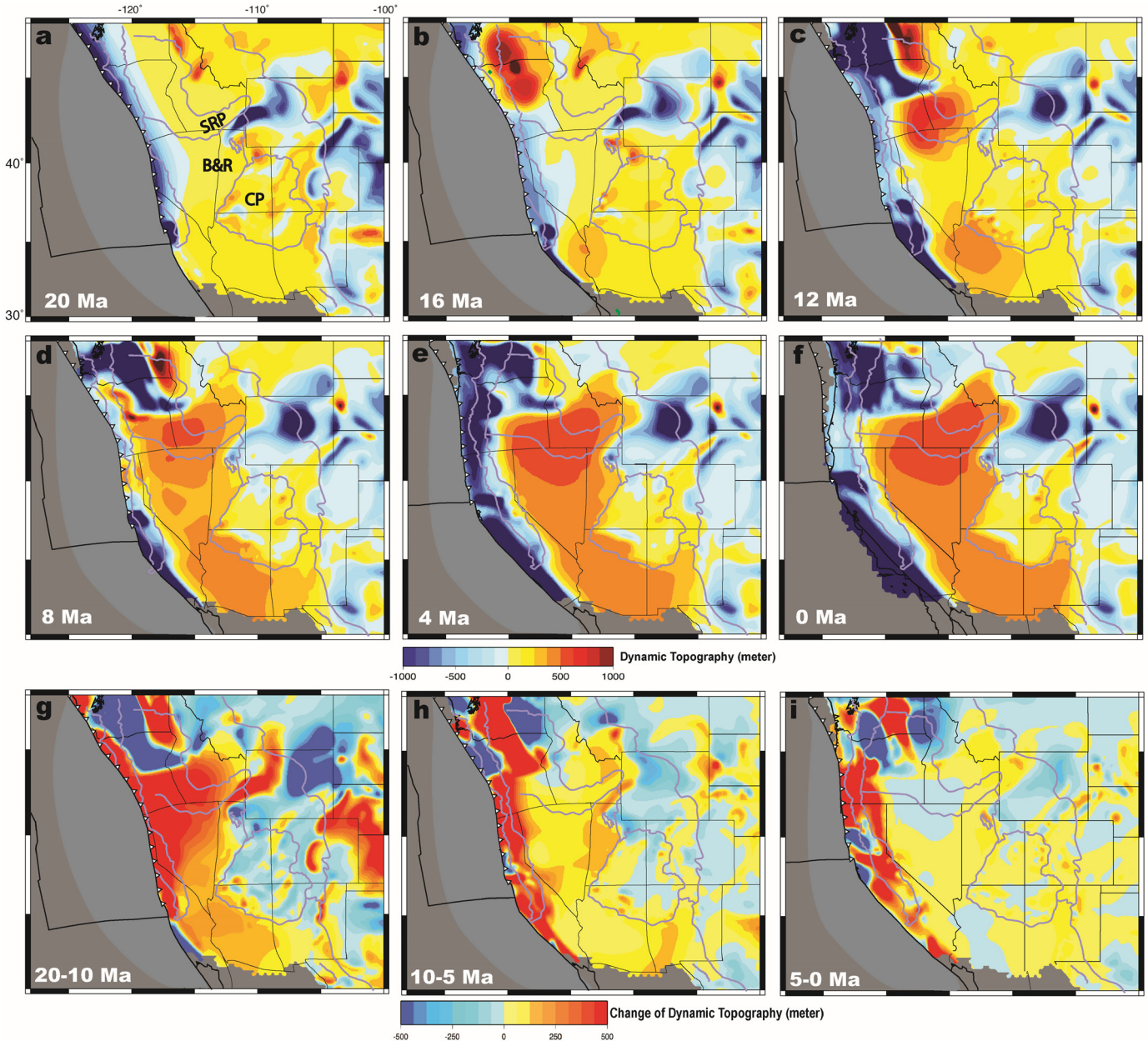

Fig. 5. Predicted history of dynamic topography and its change over time from the hybrid geodynamic model (Zhou et al., 2018a). The B&R and SRP have experienced a topographic increase with the intrusion of hot anomalies since 20 Ma (**a–f**), where the fast topography increase in this region mostly occurred before 10 Ma (**g–i**). The interior of the CP and cratonic North America has been overall stable over time. Palinspastic restoration for the outline of tectonic provinces and political states is based on Bahadori et al. (2018).

the Pacific hot mantle also occurred along the southern slab edge, causing the southern B&R to uplift.

By 12 Ma, both the hot mantle (Fig. 6c) and the associated uplift migrated into the western SRP (Fig. 5c); the disrupted subduction system accumulated large volumes of dense slab material to the north, leading the prominent subsidence in the previous CRB region. It's worth noting that the prominent dynamic topography high over SRP and northern B&R formed largely by 12 Ma (Fig. 5c, d, g), accompanying the arrival of the hot mantle (Fig. 6c, d). Since then, the areas of dynamic uplift gradually expanded eastward along the SRP toward Yellowstone and southward within the southern B&R (Fig. 5c–f), following the progressive migration of the hot mantle (Figs. 6c–f, 7). By the present-day, the SRP region has dynamically uplifted by ∼0.8 km and the B&R has uplifted by ∼0.5 km (Fig. 5a vs. 5f). During this history, the CP and other cratonic regions remain largely stable. One exception is the WY region that subsides over time, and this is due to the presence of assumed active downwelling below the region (Zhou et al., 2018a; Fig. 7).

3.4. Estimated paleotopography since the Miocene

In order to compare the model results with available observational constraints on the temporal evolution of the western U.S. topography, we construct a series of paleotopography maps by combining our dynamic topography predictions (Fig. 5) with a recent estimate on the isostatic topographic variation (Fig. S2) associated with the B&R extension that accounts for both crustal and lithospheric evolution (Bahadori et al., 2018). In accordance with the spatial coverage of mapped crustal kinematics in McQuarrie and Wernicke (2005), we limit the range of the paleotopography maps to the south of latitude 45°N, where the history of B&R extension was compiled. In this reconstruction, we neglect possible

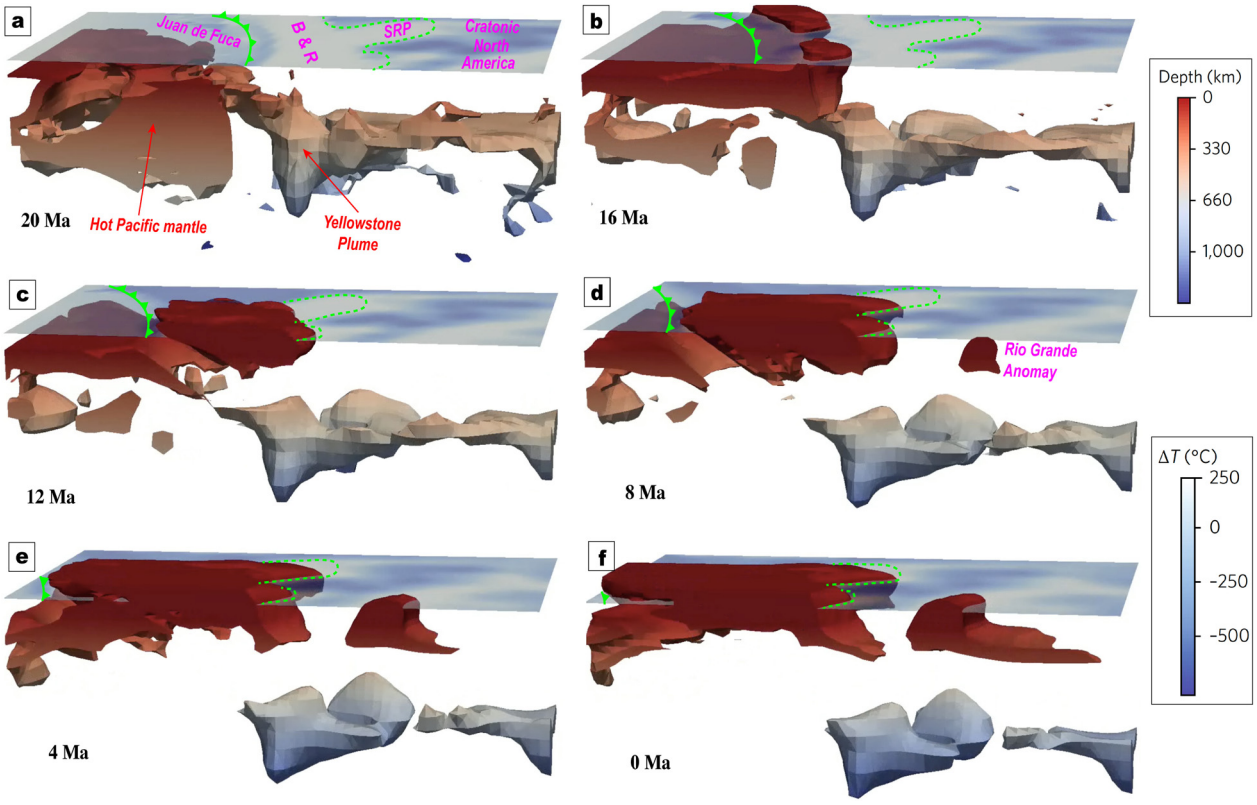

Fig. 6. 3D view of mantle evolution in the hybrid model, outlining the northern half of the mantle below the western U.S. Both an isosurface (at a temperature of +50 °C relative to the ambient mantle, with color indicating depth) and the temperature at 60-km depth (the translucent map slice, with color indicating temperature) are shown. At 20 Ma (**a**) all the hot anomalies were under the Pacific Ocean. The first pulse of hot mantle entered the western United States through the slab tear below Oregon (**b**). Subsequently the hot mantle intruded progressively into the SRP (**c**–**f**). The Yellowstone plume remained at greater depth, with its root sinking downward towards the present day.

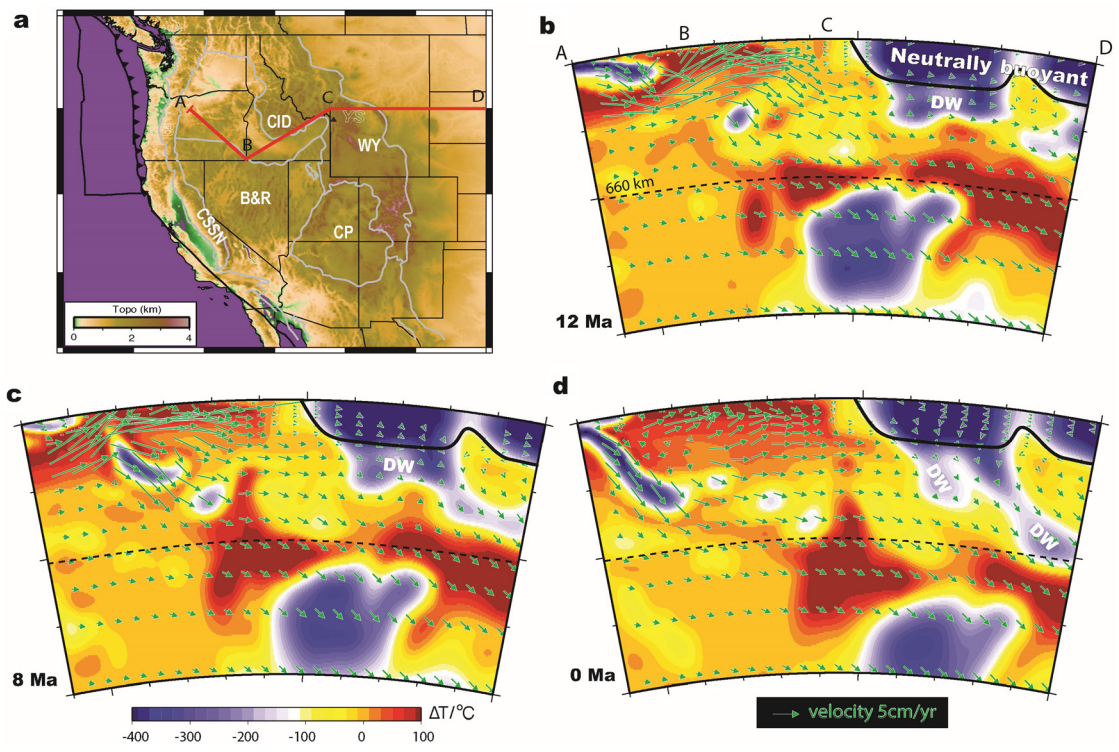

Fig. 7. (**a**) Western U.S. topography and surface location of cross section ABCD. Locations where paleoaltimetry proxies are available are also marked: CID – Central Idaho, CSSN – South-Central Sierra Nevada, CP – Colorado Plateau, B&R – Basin & Range. (**b**–**d**) Evolution of mantle thermal structure and flow field along profile ABCD from 12 Ma to the present. The eastward advancing hot mantle and its encroachment into the neutrally buoyant cratonic lithosphere (above the dark line) have caused the time-progressive Yellowstone hotspot track (Zhou et al., 2018a) and dynamically uplifted the SRP (Fig. 5). The assumed cold downwelling (DW) at the base of the Wyoming craton causes the surface to subsidence dynamically (Fig. 5).

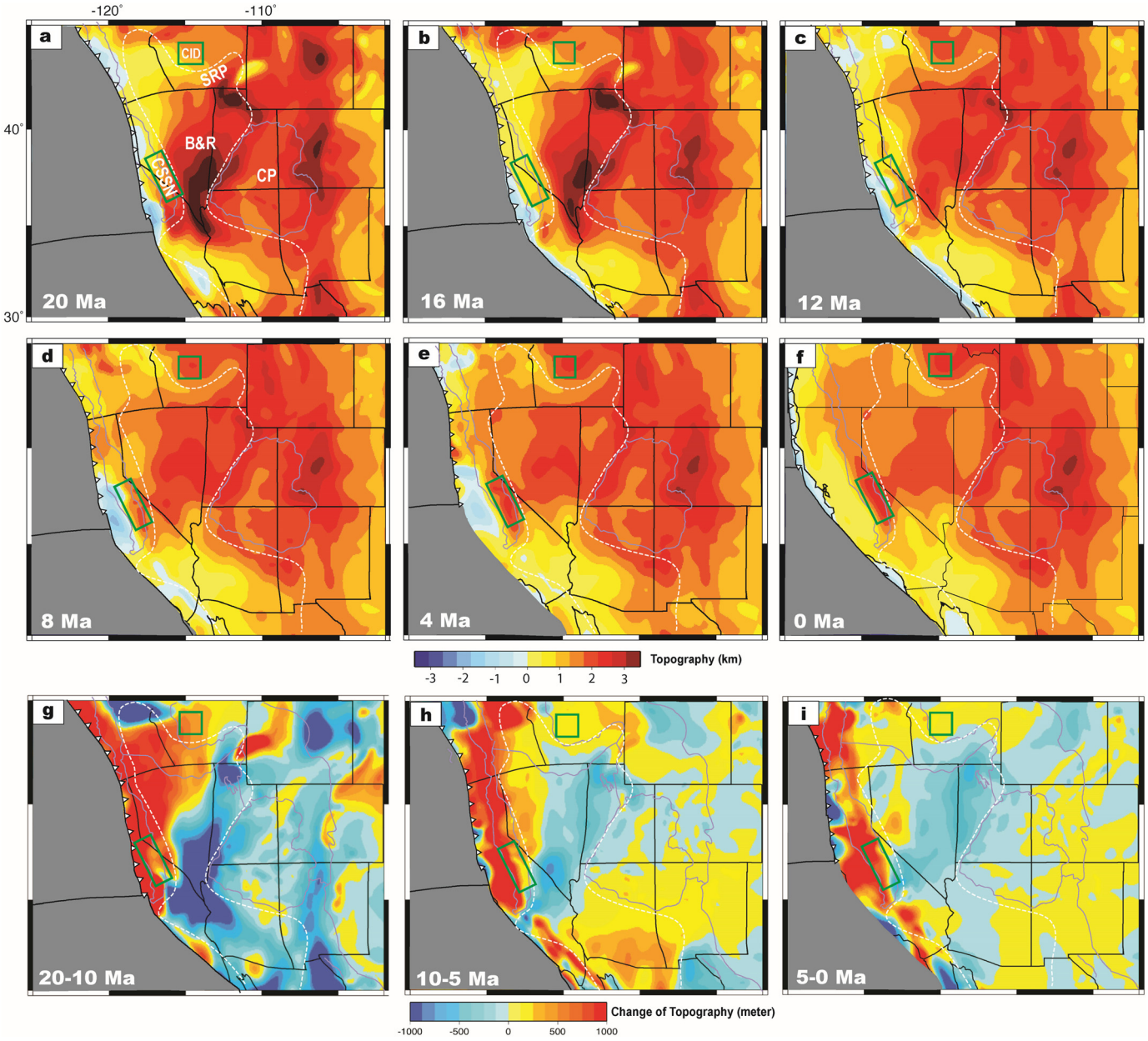

Fig. 8. Estimated paleotopography of the western U.S. since 20 Ma by combining dynamic topography with topography changes due to lithospheric isostasy. The thin white dashed line marks the tectonically active region, mainly the B&R, with the northern edge being the SRP. The green square in central Idaho indicates the location of a recent geomorphological study for paleoaltimetry (Larimer et al., 2018). The green rectangle tracks the location of CSSN over time.

topographic contributions from the compositional layering and/or delamination of mantle lithosphere as recently proposed for cratons (Hu et al., 2018).

Fig. 8 shows the estimated topographic evolution of the western U.S. since 20 Ma. A prominent feature is the declining topography within the central-eastern B&R with a total magnitude of −1.5 km since the middle Miocene (Fig. 8a–f). This is dominantly due to crustal thinning that results in a topographic decrease of ∼−2 km (Fig. S2), as the relatively minor topographic increase (∼0.5 km) due to dynamic topography prior to 5 Ma (Fig. 5) does not reverse the monotonic subsidence in the region (Fig. 8g–i). In contrast, the western B&R and the SRP have experienced continuous uplift of 1 km since 20 Ma, mostly reflecting dynamic topography due to the intruding hot mantle. According to these maps, the regions to the east of the B&R experience little to no uplift during this history; however, as discussed later, this part of the model still needs more work. Within stable North America, one location that did experience significant dynamic uplift is the region north of the SRP, particularly in Idaho, which has been uplifted by ∼1 km since ∼12 Ma. This is when the hot Pacific mantle arrived underneath and has occupied the asthenosphere since then (Fig. 6).

4. Discussion and conclusion

In this paper, we investigate the origin and evolution of the high western U.S. topography by analyzing gravity, residual topography and geodynamic modeling. If the observed surface topography is isostatically supported within the crust or the lithosphere, the resulting free air gravity anomaly should be close to zero. However, both the rapidly varying crustal (lithospheric) thickness within the western U.S. and the existence of uncompensated deep buoyancy would lead to large gravity anomalies. This phenomenon provides an effective constraint on the degree of isostatic compensation of the western U.S. topography. While attributing all surface

topography variations to shallow (lower crust) density anomalies severely violates both the gravity and density constraints, putting the mass anomalies at greater depths helps to better match gravity (Fig. 2f vs. Fig. 3e), but still with unrealistically low density of the lithosphere below the western U.S. Both these isostasy calculations require additional buoyant asthenosphere beneath the thin lithosphere of the B&R province (Figs. 2f, 3d–f). This conclusion is also potentially consistent with assuming isostatic compensation at a constant 150 km depth as adopted in Levandowski et al. (2014), where the buoyant asthenosphere below the western U.S. is considered as part of the isostatic system. Our gravity analysis, therefore, reconciles the two recent studies by Becker et al. (2014) and Levandowski et al. (2014), with the former assuming a variable LAB depth.

We emphasize that, compared to the tectonically active SRP and B&R whose topography is dynamically supported by the underlying mantle, the density structure and mantle dynamics below the stable portion of the western U.S. (CP, WY, etc.) are less well constrained. The fact that both residual topography (Fig. 4) and dynamic topography (Fig. 5) are negative over these regions seems to imply that the seismically observed sub-lithospheric fast anomalies beneath the region (Schmandt and Lin, 2014) represent high-density anomalies. However, the mantle residual gravity over these stable regions (Fig. 3d, e) does not show prominent positive signals, contrary to the presence of high-density upper mantle materials. This dilemma likely results from either inaccurate lithosphere depth or uncertain mantle density below this region. Therefore, we conclude that without considering more data constraints, one cannot uniquely map out the density profile of the seismically fast mantle anomalies below the stable part of the western U.S. (e.g., shown in Fig. 7d).

A unique result of this study is the positive dynamic topography over the tectonically active western U.S. According to our geodynamic model, the B&R and the SRP experienced progressively increasing dynamic uplift since the early Miocene (Fig. 5) due to the lateral intrusion of hot Pacific mantle into the continental interior (Fig. 6). This, when combined with the contribution from lithospheric isostasy, results in prominent elevation gain along the west coast and the SRP but continuous elevation decrease further east due to the dominant effect of crustal extension (Fig. 8).

The incremental dynamic uplift amounting to ~2 km from 20 Ma to the present along the central-southern Sierra Nevada (CSSN) explains the episodic mid-late Miocene uplift events of the central Sierra Nevada inferred from volcanic stratigraphy, which provides the timing but not amplitudes of uplift (Hagan et al., 2009; Fig. 9). The prominent late Miocene (5–2 Ma) uplift with a magnitude of ~1 km within southern Sierra Nevada (Fig. 9) is associated with the convective removal of a piece of accreted slab and infill of hot asthenospheric mantle (Liu and Stegman, 2011; Zhou et al., 2018a; Figs. 6, 7). This scenario is consistent with the 4-Ma magmatic flare-up event at this location (McQuarrie and Oskin, 2010). To the north of the SRP, the geomorphological evolution of the Idaho batholith reveals an abrupt base-level change starting around 13–8 Ma, implying a km-scale uplift in central Idaho (Larimer et al., 2018). This inference is in remarkable consistency with our modeled dynamic uplift history where an abrupt uplift occurred at 14–11 Ma in the same region that leads to a total of ~800 m elevation gain by the present day (Figs. 5, 8, 9).

It is generally challenging to infer the past elevation of tectonically active regions. A recent study analyzing oxygen isotopes over the Great Basin concluded a significant (>1 km) topographic decrease since the middle Miocene (Horton et al., 2004). This result is consistent with our modeled continuous subsidence with a total magnitude of 1 km within most of the B&R (Fig. 8), mainly as a result of crustal extension. Further east, the CP and WY regions experienced little dynamic uplift (Fig. 5), due to the lack of mantle upwelling underneath (Figs. 6, 7, 9). This result differs from earlier modeling studies that suggest late-Cenozoic dynamic uplift of the CP (e.g., Moucha et al., 2009). On the other hand, the lack of recent uplift at the interior of the CP (Fig. 9) and areas beyond (Fig. 8) is in line with the paleo-altimetry inference based on paleo-botany (Wolfe et al., 1998) that argues for a high Oligocene topography in these regions. This model result is also consistent a recent carbonate clumped isotope analysis suggesting little uplift of the CP since 20 Ma (Huntington et al., 2010; Fig. 9). We caution that the paleotopography of the tectonically active regions surrounding the CP, such as the Rio Grande and the Rockies, is subject to future research, since the model dynamics for these locations was less well constrained.

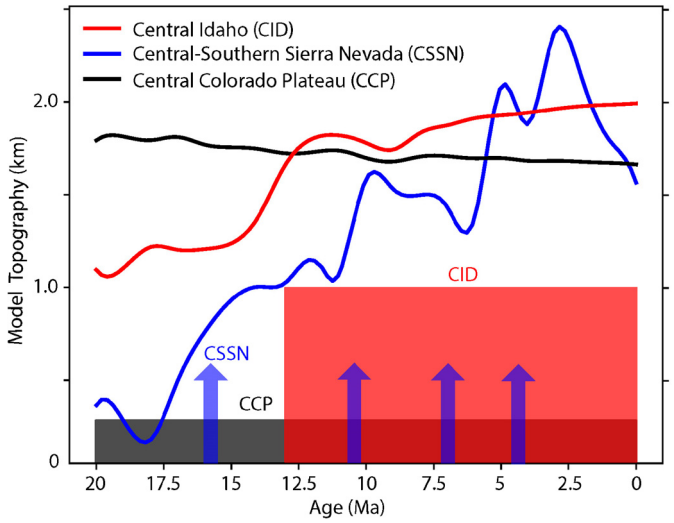

Fig. 9. Modeled (lines) and observed (filled symbols) uplift histories at three localities within the western U.S. The locations of these paleoaltimetry estimates are shown in Fig. 7. The three colored lines mark the modeled topography. The red box represents the geomorphologically inferred km-scale uplift in central Idaho (Larimer et al., 2018). The blue arrows mark the episodic uplift events inferred from volcanic stratigraphy with unknown amplitudes of uplift (Hagan et al., 2009; McQuarrie and Oskin, 2010).

We conclude that the tectonically active B&R and the SRP has experienced dynamic uplift by 0.5–1 km since the Early Miocene, as a result of the eastward intrusion of the hot Pacific mantle below the region. However, crustal extension within the B&R caused the elevation to decrease isostatically, leading to net subsidence within most of the eastern B&R province. The estimated topographic evolution within the western U.S. matches several paleoaltimetry observations. Physically, this model is consistent with constraints not only from gravity (this study) and residual topography (Becker et al., 2014), but also the region's seismic anisotropy (Zhou et al., 2018b) and intraplate volcanism (Zhou et al., 2018a). According to this model, the cratonic part of the continent acquired little dynamic uplift since 20 Ma, due to the lack of mantle upwelling from underneath (Figs. 6, 7). Therefore, if uplift did occur during this period (e.g., Karlstrom et al., 2012), processes other than deep mantle upwelling must be taken into account.

Acknowledgements

We thank Nicolas Flament and Will Levandowski for their constructive review of this work. We thank Bill Holt for sharing their reconstructed history of the isostatic topography maps of the western U.S. The numerical models were performed using CitcomS (www.geodynamics.org) and GPlates (www.gplates.org). Figures were prepared using the GMT software package (https://www.soest.hawaii.edu/gmt/). L.L. thanks NSF support through grants EAR-1345135 and 1554554. This research is part of the Blue Wa-

ters sustained-petascale computing project, which is supported by the National Science Foundation (awards OCI-0725070 and ACI-1238993) and the state of Illinois. Blue Waters is a joint effort of the University of Illinois at Urbana-Champaign and its National Center for Supercomputing Applications. This work is also part of the "PRAC Title 4-D Geodynamic Modeling With Data Assimilation: Origin Of Intra-Plate Volcanism In The Pacific Northwest" PRAC allocation support by the National Science Foundation (award number ACI 1516586). This work also used the Extreme Science and Engineering Discovery Environment (XSEDE), which is supported by National Science Foundation grant number ACI-1548562.

Appendix A. Supplementary material

Supplementary material related to this article can be found online at https://doi.org/10.1016/j.epsl.2019.02.029.

References

Bahadori, A., Holt, W.E., Rasbury, E.T., 2018. Reconstruction modeling of crustal thickness and paleotopography of western North America since 36 Ma. Geosphere 14. https://doi.org/10.1130/GES01604.1.

Becker, T.W., Faccenna, C., Humphreys, E.D., Lowry, A.R., Miller, M.S., 2014. Static and dynamic support of western United States topography. Earth Planet. Sci. Lett. 402, 234–246.

Braun, J., 2010. The many surface expressions of mantle dynamics. Nat. Geosci. 3, 825–833.

Bunge, H.P., Hagelberg, C.R., Travis, B.J., 2003. Mantle circulation models with variational data assimilation: inferring past mantle flow and structure from plate motion histories and seismic tomography. Geophys. J. Int. 152 (2), 280–301.

Carlson, R.L., Johnson, H.P., 1994. On modeling the thermal evolution of the oceanic upper mantle: an assessment of the cooling plate model. J. Geophys. Res., Solid Earth 99 (B2), 3201–3214.

Carlson, R.W., Pearson, D.G., James, D.E., 2005. Physical, chemical, and chronological characteristics of continental mantle. Rev. Geophys. 43, RG1001.

DeNosaquo, K.R., Smith, R.B., Lowry, A.R., 2009. Density and lithospheric strength models of the Yellowstone–Snake River Plain volcanic system from gravity and heat flow data. J. Volcanol. Geotherm. Res. 188 (1–3), 108–127.

Flament, N., Gurnis, M., Müller, R.D., 2013. A review of observations and models of dynamic topography. Lithosphere 5 (2), 189–210.

Flowers, R.M., 2010. The enigmatic rise of the Colorado Plateau. Geology 38 (7), 671–672.

Forte, A.M., Moucha, R., Simmons, N.A., Grand, S.P., Mitrovica, J.X., 2010. Deep-mantle contributions to the surface dynamics of the North American continent. Tectonophysics 481 (1–4), 3–15.

Griffin, W.L., O'Reilly, S.Y., Doyle, B.J., Pearson, N.J., Coopersmith, H., Kivi, K., Pokhilenko, N., 2004. Lithosphere mapping beneath the North American plate. Lithosphere 77, 873–922.

Hagan, J.C., Busby, C.J., Putirka, K., Renne, P.R., 2009. Cenozoic palaeocanyon evolution, ancestral Cascades arc volcanism, and structure of the Hope Valley–Carson Pass region, Sierra Nevada, California. Int. Geol. Rev. 51 (9–11), 777–823.

Hager, B.H., Richards, M.A., 1989. Long-wavelength variations in Earth's geoid – physical models and dynamical implications. Philos. Trans. R. Soc. Lond. A 328, 309–327.

Hansen, S.M., Dueker, K., Schmandt, B., 2015. Thermal classification of lithospheric discontinuities beneath USArray. Earth Planet. Sci. Lett. 431, 36–47.

Hasterok, D., Chapman, D.S., 2007. Continental thermal isostasy: 2. Application to North America. J. Geophys. Res., Solid Earth 112, B06415.

Hoggard, M.J., White, N., Al-Attar, D., 2016. Global dynamic topography observations reveal limited influence of large-scale mantle flow. Nat. Geosci. 9 (6), 456.

Hoggard, M.J., Winterbourne, J., Czarnota, K., White, N., 2017. Oceanic residual depth measurements, the plate cooling model, and global dynamic topography. J. Geophys. Res., Solid Earth 122 (3), 2328–2372.

Horton, T.W., Sjostrom, D.J., Abruzzese, M.J., Poage, M.A., Waldbauer, J.R., Hern, M., Wooden, J., Chamberlain, C.P., 2004. Spatial and temporal variation of Cenozoic surface elevation in the Great Basin and Sierra Nevada. Am. J. Sci. 304, 862–888.

Hu, J., Liu, L., Faccenda, M., Zhou, Q., Fischer, K.M., Marshak, S., Lundstrom, C., 2018. Modification of the Western Gondwana craton by plume–lithosphere interaction. Nat. Geosci. 11 (3), 203.

Huntington, K.W., Wernicke, B.P., Eiler, J.M., 2010. The influence of climate change and uplift on Colorado Plateau paleotemperatures from carbonate clumped-isotope thermometry. Tectonics 29, TC3005.

Karlstrom, K.E., Coblentz, D., Dueker, K., Ouimet, W., Kirby, E., Van Wijk, J., Schmandt, B., Kelley, S., Lazear, G., Crossey, L.J., Crow, R., 2012. Mantle-driven dynamic uplift of the Rocky Mountains and Colorado Plateau and its surface response: toward a unified hypothesis. Lithosphere 4 (1), 3–22.

Larimer, J.E., Yanites, B.J., Phillips, W., Mittelstaedt, E., 2018. Late Miocene rejuvenation of central Idaho landscape evolution: a case for surface processes driven by plume–lithosphere interaction. Lithosphere. https://doi.org/10.1130/L746.1.

Levandowski, W., Jones, C.H., Shen, W., Ritzwoller, M.H., Schulte-Pelkum, V., 2014. Origins of topography in the western US: mapping crustal and upper mantle density variations using a uniform seismic velocity model. J. Geophys. Res., Solid Earth 119 (3), 2375–2396.

Lithgow-Bertelloni, C., Silver, P.G., 1998. Dynamic topography, plate driving forces and the African superswell. Nature 395, 269–272.

Liu, L., 2015. The ups and downs of North America: evaluating the role of mantle dynamic topography since the Mesozoic. Rev. Geophys. 53 (3), 1022–1049.

Liu, L., Gurnis, M., 2008. Simultaneous inversion of mantle properties and initial conditions using an adjoint of mantle convection. J. Geophys. Res., Solid Earth 113 (B8).

Liu, L., Gurnis, M., 2010. Dynamic subsidence and uplift of the Colorado Plateau. Geology 38 (7), 663–666.

Liu, L., Stegman, D.R., 2011. Segmentation of the Farallon slab. Earth Planet. Sci. Lett. 311, 1–10.

Liu, L., Hasterok, D., 2016. High-resolution lithosphere viscosity and dynamics revealed by magnetotelluric imaging. Science 353 (6307), 1515–1519.

McCurry, M., Rodgers, D.W., 2009. Mass transfer along the Yellowstone hotspot track I: petrologic constraints on the volume of mantle-derived magma. J. Volcanol. Geotherm. Res. 188 (1), 86–98.

McQuarrie, N., Wernicke, B.P., 2005. An animated tectonic reconstruction of southwestern North America since 36 Ma. Geosphere 1, 147–172.

McQuarrie, N., Oskin, M., 2010. Palinspastic restoration of NAVDat and implications for the origin of magmatism in southwestern North America. J. Geophys. Res., Solid Earth 115, B10401.

Molnar, P., England, P.C., Jones, C.H., 2015. Mantle dynamics, isostasy, and the support of high terrain. J. Geophys. Res., Solid Earth 120, 1932–1957.

Moucha, R., Forte, A.M., Rowley, D.B., Mitrovica, J.X., Simmons, N.A., Grand, S.P., 2009. Deep mantle forces and the uplift of the Colorado Plateau. Geophys. Res. Lett. 36 (19).

Müller, R.D., Sdrolias, M., Gaina, C., Roest, W.R., 2008. Age, spreading rates, and spreading asymmetry of the world's ocean crust. Geochem. Geophys. Geosyst. 9 (4).

Pasyanos, M.E., Masters, T.G., Laske, G., Ma, Z., 2014. LITHO1.0: an updated crust and lithospheric model of the Earth. J. Geophys. Res., Solid Earth 119, 2153–2173.

Schmandt, B., Humphreys, E., 2011. Seismically imaged relict slab from the 55 Ma Siletzia accretion to the northwest United States. Geology 39, 175–178.

Schmandt, B., Lin, F.C., 2014. P and S wave tomography of the mantle beneath the United States. Geophys. Res. Lett. 41 (18), 6342–6349.

Schmandt, B., Lin, F.C., Karlstrom, K.E., 2015. Distinct crustal isostasy trends east and west of the Rocky Mountain Front. Geophys. Res. Lett. 42 (23).

Sigloch, K., 2011. Mantle provinces under North America from multifrequency P wave tomography. Geochem. Geophys. Geosyst. 12 (2).

Wolfe, J.A., Forest, C.E., Molnar, P., 1998. Paleobotanical evidence of Eocene and Oligocene paleoaltitudes in midlatitude western North America. Geol. Soc. Am. Bull. 110, 664–678.

Yang, T., Gurnis, M., 2016. Dynamic topography, gravity and the role of lateral viscosity variations from inversion of global mantle flow. Geophys. Suppl. Mon. Not. R. Astron. Soc. 207 (2), 1186–1202.

Yang, T., Moresi, L., Müller, R.D., Gurnis, M., 2017. Oceanic residual topography agrees with mantle flow predictions at long wavelengths. Geophys. Res. Lett. 44 (21).

Zhou, Q., Liu, L., 2017. A hybrid approach to data assimilation for reconstructing the evolution of mantle dynamics. Geochem. Geophys. Geosyst. 18 (11), 3854–3868.

Zhou, Q., Liu, L., Hu, J., 2018a. Western US volcanism due to intruding oceanic mantle driven by ancient Farallon slabs. Nat. Geosci. 11 (1), 70.

Zhou, Q., Hu, J., Liu, L., Chaparro, T., Stegman, D.R., Faccenda, M., 2018b. Western US seismic anisotropy revealing complex mantle dynamics. Earth Planet. Sci. Lett. 500, 156–167.